Anomalous magnetothermoelectric behavior in massive Dirac materials

Yanan Li,[1,2] Huichao Wang,[3] Jingyue Wang,[4,5] Chunming Wang,[6,7] Yanzhao Liu,[1] Jun Ge,[1] Jingjing Niu,[4] Wenjie Zhang,[4] Pinyuan Wang,[1] Ran Bi,[4] Jinglei Zhang,[8] Ji-Yan Dai,[9] Jiaqiang Yan,[10] David Mandrus,[10,11] Nitin Samarth,[2] Haizhou Lu,[7,12,*] Xiaosong Wu,[4,13,†] and Jian Wang[1,7,14,15,16,17,‡]

[1]*International Center for Quantum Materials, School of Physics, Peking University, Beijing 100871, China*
[2]*Department of Physics, The Pennsylvania State University, University Park, Pennsylvania 16802, USA*
[3]*School of Physics, Sun Yat-sen University, Guangzhou 510275, China*
[4]*State Key Laboratory for Artificial Microstructure and Mesoscopic Physics, Peking University, Beijing 100871, China*
[5]*Center for Nanochemistry, Beijing Science and Engineering Center for Nanocarbons, Beijing National Laboratory for Molecular Sciences, College of Chemistry and Molecular Engineering, Peking University, Beijing 100871, China*
[6]*Department of Physics, Shanghai Normal University, Shanghai 200234, China*
[7]*Institute for Quantum Science and Engineering and Department of Physics, Southern University of Science and Technology, Shenzhen 518055, China*
[8]*High Magnetic Field Laboratory, Chinese Academy of Sciences, Hefei 230031, Anhui, China*
[9]*Department of Applied Physics, The Hong Kong Polytechnic University, Hung Hom, Kowloon, Hong Kong, China*
[10]*Materials Science and Technology Division, Oak Ridge National Laboratory, Oak Ridge, Tennessee 37831, USA*
[11]*Department of Materials Science and Engineering, University of Tennessee, Knoxville, Tennessee 37996, USA*
[12]*Shenzhen Key Laboratory of Quantum Science and Engineering, Shenzhen 518055, China*
[13]*Beijing Key Laboratory of Quantum Devices, Peking University, Beijing 100871, China*
[14]*Collaborative Innovation Center of Quantum Matter, Beijing 100871, China*
[15]*CAS Center for Excellence in Topological Quantum Computation, University of Chinese Academy of Sciences, Beijing 100190, China*
[16]*Beijing Academy of Quantum Information Sciences, Beijing 100193, China*
[17]*Hefei National Laboratory, Hefei 230088, China*

(Received 1 January 2022; revised 2 February 2023; accepted 6 February 2023; published 23 February 2023)

Extensive studies of electron transport in Dirac materials have shown positive magnetoresistance (MR) and positive magnetothermopower (MTP) in a magnetic field perpendicular to the excitation current or thermal gradient. In contrast, measurements of electron transport often show a negative longitudinal MR and negative MTP for a magnetic field oriented along the excitation current or thermal gradient; this is attributed to the chiral anomaly in Dirac materials. Here, we report a very different magnetothermoelectric transport behavior in the massive Dirac material $ZrTe_5$. Although thin flakes show a commonly observed positive MR in a perpendicular magnetic field, distinct from other Dirac materials, we observe a sharp negative MTP. In a parallel magnetic field, we still observe a negative longitudinal MR, however, a remarkable positive MTP is observed for the fields parallel to the thermal gradients. Our theoretical calculations suggest that this anomalous magnetothermoelectric behavior can be attributed to the screened Coulomb scattering. This work demonstrates the significance of impurity scattering in the electron transport of topological materials and provides deep insight into the magnetotransport phenomena in Dirac materials.

DOI: 10.1103/PhysRevB.107.085140

I. INTRODUCTION

Electrical and thermoelectric transport studies of Dirac materials are gaining increasing attention as a powerful tool to reveal the underlying physics, including the scattering mechanism, band structure, and topology. The experimental studies of Dirac materials, such as the Dirac semimetal Cd_3As_2 [1], the Weyl semimetal GdPtBi [2], and the massive Dirac material $Pb_{1-x}Sn_xSe$ [3], demonstrate that both the magnetothermopower (MTP) and magnetoresistance (MR) increase with an increasing perpendicular magnetic field (B) [1–4], while they decrease with an increasing parallel field owing to the chiral anomaly [1,2]. The classical magnetoelectric conductivity under a perpendicular magnetic field is given by the Boltzmann-Drude model: $\sigma(B) = \frac{en\mu}{(1+\mu^2B^2)}$. Here, n is the carrier density; μ is the mobility with $\mu = \tau(E)/m$ where m is the effective mass and $\tau(E)$ is the relaxation time. According to the Mott relation [5], the Seebeck coefficient can be written as $S = -\frac{\pi^2k_B^2T}{3e}\left(\frac{\partial \ln\sigma(E)}{\partial E}\right)_{E_F}$, where $-e$ is the electron charge, k_B is the Boltzmann constant, T is the temperature, σ is the electric conductivity, and E_F is the Fermi level. Therefore, the detailed behavior of MTP with magnetic field (i.e., whether it increases or decreases with field) is affected by the energy dependence of the relaxation time ($\tau(E)$), which depends on the impurity scattering in the system.

*luhz@sustech.edu.cn
†xswu@pku.edu.cn
‡jianwangphysics@pku.edu.cn

The fundamental understanding of impurity scattering in topological materials has been a subject of intense scientific interest. In topological insulators, impurities lead to intricate effects on both the bulk and surface properties. For example, they can modify the electrical transport [6] or induce nanoscale spatial fluctuations in the helicity of surface states [7]. In topological semimetals, the electrical conductivity can also be tuned by impurities, resulting in diverse magnetic field dependent behavior [8–13]. Recently, there has been growing interest in the thermoelectric properties of topological materials in the presence of different charge-impurity scattering mechanisms [14–19]. The thermoelectric behavior is dramatically influenced by the scattering potential and thus may reveal the nature of different scattering mechanisms in topological materials.

Among topological materials, the massive Dirac material $ZrTe_5$ [20–22] has been a very promising platform to explore novel quantum effects because of its small Fermi surface [23–26]. Usually, $ZrTe_5$ can reach the quantum limit at a low magnetic field, which enables the discovery of many exotic quantum phenomena, such as the log B periodic quantum oscillations [27–29], the three-dimensional quantum Hall effect [30], and quantized plateau in the thermoelectric Hall conductivity [31]. Additionally, experiments have also shown anomalous transport behaviors, such as a negative longitudinal MR [32], an anomalous Hall effect [33–35], and an unconventional Hall effect [36], implying the nontrivial topological band structure of $ZrTe_5$.

In this work, we present experimental studies of combined magnetoelectrical and magnetothermoelectric transport in $ZrTe_5$ thin flakes with dominant hole carriers at low temperatures. The MR shows a magnetic field dependence that is qualitatively similar to that observed in other Dirac materials but the thermoelectric behavior shows a field dependence distinct from that seen in previous studies of Dirac materials. When the magnetic field is perpendicular to the thermal gradient, we observe a negative MTP that saturates in the high field regime. In addition, a positive MTP is detected when the magnetic field is parallel to the thermal gradient. Our theoretical analyses indicate that this distinct MTP behavior can be attributed to the dominant long-range screened Coulomb scattering in these crystals. Our observations are highly valuable for understanding the quantum transport phenomena in Dirac materials.

II. METHODS

$ZrTe_5$ flakes were exfoliated with Scotch tape method and transferred onto SiO_2/Si substrates. Then they were spin coated with photoresists. After that, standard electron beam lithography, development, and metal evaporation were carried out to generate the electrodes and on-chip heater. For devices used in thermoelectric transport measurements, Pd (6.5 nm)/Au (40 nm) was used for the heater, and Pd (6.5 nm)/Au (300 nm) was used for other electrodes.

The temperature difference throughout the sample can be measured by the fabricated Pd/Au thermometers on top of the two ends of the thin flakes. The heat is generated by the on-chip microheater. In the device, two ends of the nanoflake are sandwiched between the substrate and gold stripes serving as thermometers [Fig. S1 of the Supplemental Material [41] and Fig. 1(b)]. It is reasonable to believe that the substrate, nanoflake, and gold stripe are in thermal equilibrium at these two locations. Therefore, the temperature of the thermometer is indeed the temperature of the sample and the substrate. The measured temperature difference across the nanoflake in this configuration is relatively accurate. During the experiment, we made sure that this temperature difference was always much smaller than the average temperature of the flake. The thermopower can be considered as a constant across the sample and thus can be calculated by the thermoelectric voltage divided by the temperature difference. Under this condition, there is no need to take into account the actual temperature distribution between two thermometers. This setup is commonly used for measuring thermopower of mesoscopic samples, such as carbon nanotubes [37], graphene [38], and topological semimetals [1,39].

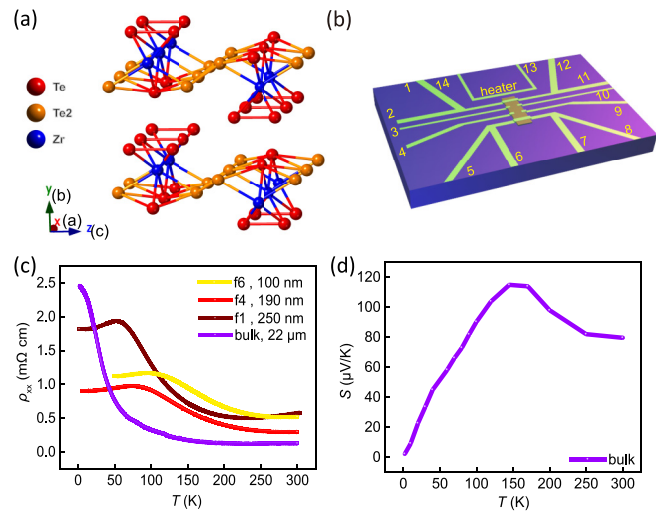

FIG. 1. Temperature dependence of the resistivity and thermopower in $ZrTe_5$. (a) Crystal structure of $ZrTe_5$. (b) Schematic of the measurement configuration of $ZrTe_5$ thin flakes. Contacts 1, 2, 11, and 12 and contacts 5, 6, 7, and 8 are used to inject an excitation current or measure the temperature at the two ends of the sample. Contacts 3, 4, 9, and 10 are used to measure the MR and Hall signals in a standard Hall-bar setup. Contacts 2 and 5 or contacts 11 and 8 are used to measure the thermoelectric voltage. Contact 13 and 14 are used to apply a voltage on the heater to generate a thermal gradient on the sample. (c) The resistivity vs temperature curves of the $ZrTe_5$ bulk crystal and thin flakes with different thicknesses. (d) Temperature dependence of the thermopower of a $ZrTe_5$ bulk crystal.

Most transport measurements were performed in a 14-T helium cryostat and a 9-T Quantum Design Physical Property Measurement System by using the lock-in method. The ultrahigh field measurements were conducted in a static magnetic field facility (33 T) at the High Magnetic Field Laboratory, Chinese Academy of Sciences at Hefei.

III. EXPERIMENTAL RESULTS

We carried out the magnetotransport measurements on $ZrTe_5$ thin flakes exfoliated from bulk crystals. Figure 1(a) shows the crystalline structure of $ZrTe_5$. Individual layers are

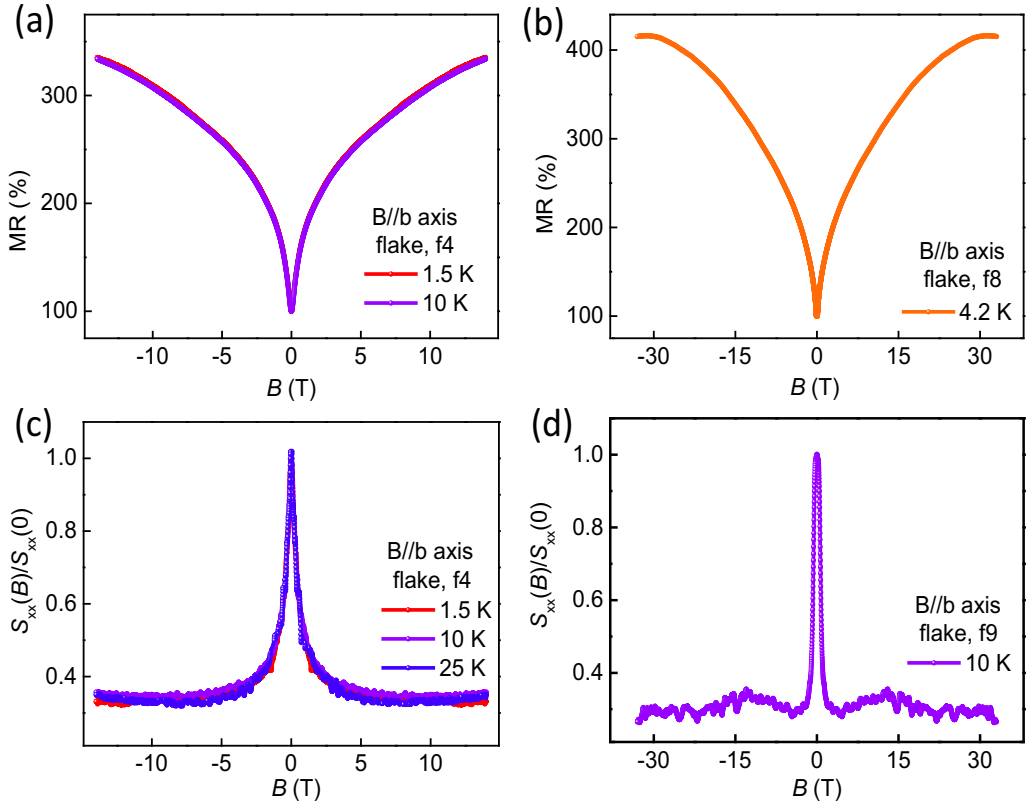

FIG. 2. Normalized MR (a),(b) and MTP (c),(d) in $ZrTe_5$ flake samples under perpendicular fields ($B//b$ axis). The MR is calculated as $\mathrm{MR} = R(B)/R(0) \times 100\%$. The MTP decreases sharply at low fields and saturates at high magnetic fields.

coupled via van der Waals interactions, stacking along the b axis. Our bulk $ZrTe_5$ crystals with a very low carrier density were grown by the Te-flux method as reported [40]. For transport measurements, we used electron beam lithography and electron beam evaporation to pattern electrodes on thin flakes. An excitation current I or a thermal gradient ∇T was applied along the a axis of $ZrTe_5$ crystals ($I//a$ or $\nabla T//a$) for electric and thermoelectric transport measurements, respectively. Figure 1(b) shows the schematic of the measurement configuration and Fig. S1(a) [41] is an optical microscopy image of a typical device. Figure 1(c) displays the ρ-T curves from 300 to 2 K for samples with different thicknesses. The exfoliated thin flakes clearly show a resistivity peak anomaly at a temperature that increases with decreasing flake thickness, similar to that in $ZrTe_5$ grown by the iodine vapor transfer (IVT) method [42]. We note that the peak anomaly is absent in the parent bulk crystals down to 2 K [Fig. 1(c)] while it usually presents in the IVT-grown bulk samples [43]. Additionally, the peak anomaly in the IVT-grown samples is usually accompanied by a change in the dominant carrier type [40]. However, this does not occur in our flux-grown samples. The different transport characteristics are likely related to the density of Te vacancies [40,44], and the flux-grown crystals contain relatively fewer Te vacancies (Fig. S8) [37,38]. Figure 1(d) is the temperature dependent thermopower of a bulk crystal. The positive thermopower of both the bulk and thin flake samples (Fig. S2 [41]) indicates the dominant carriers are holes over the temperature range 300–2 K, consistent with the Hall measurements (Figs. S3, S4, and S5 [41]). To avoid possible quality decay, the flakes were freshly cleaved and stored in an Ar glove box before measurements.

The magnetotransport behavior of thin flakes of $ZrTe_5$ was then measured by applying a perpendicular external magnetic field ($B//b$). In the electrical transport measurements, the samples show a positive MR with a sublinear field dependence [Figs. 2(a) and 2(b)], consistent with the previous reports [23,32,45,46]. Surprisingly, the magnetothermoelectric transport measurements show a negative MTP in all samples. As shown in Fig. 2(c), the thermopower decreases sharply with the applied magnetic field and eventually saturates at large fields. The negative and saturated MTP extends up to 33 T [Fig. 2(d)].

As the magnetic field orientation is tilted from the perpendicular configuration ($B//b$ axis) to the current direction ($B//a$ axis), the positive MR is first suppressed and then flips to the negative MR, as shown in Figs. 3(a) and 3(b). This behavior is further confirmed in another sample [Fig. S6(a) [41]]. The amplitude of the negative MR generally decreases with increasing temperature and vanishes at a temperature between 100 and 150 K, as shown in Fig. 3(b). The negative MTP is also suppressed when the field orientation deviates from the b axis, and a positive MTP is observed when the magnetic field is tilted to the temperature gradient direction [Figs. 3(c) and 3(d)]. The flat trace at low fields when $\theta = 90^\circ$ [Fig. 3(c)] may be due to the presence of a tiny misalignment angle in the measurement, i.e., the sharp negative MTP contribution from the perpendicular component offsets the positive MTP under the parallel field.

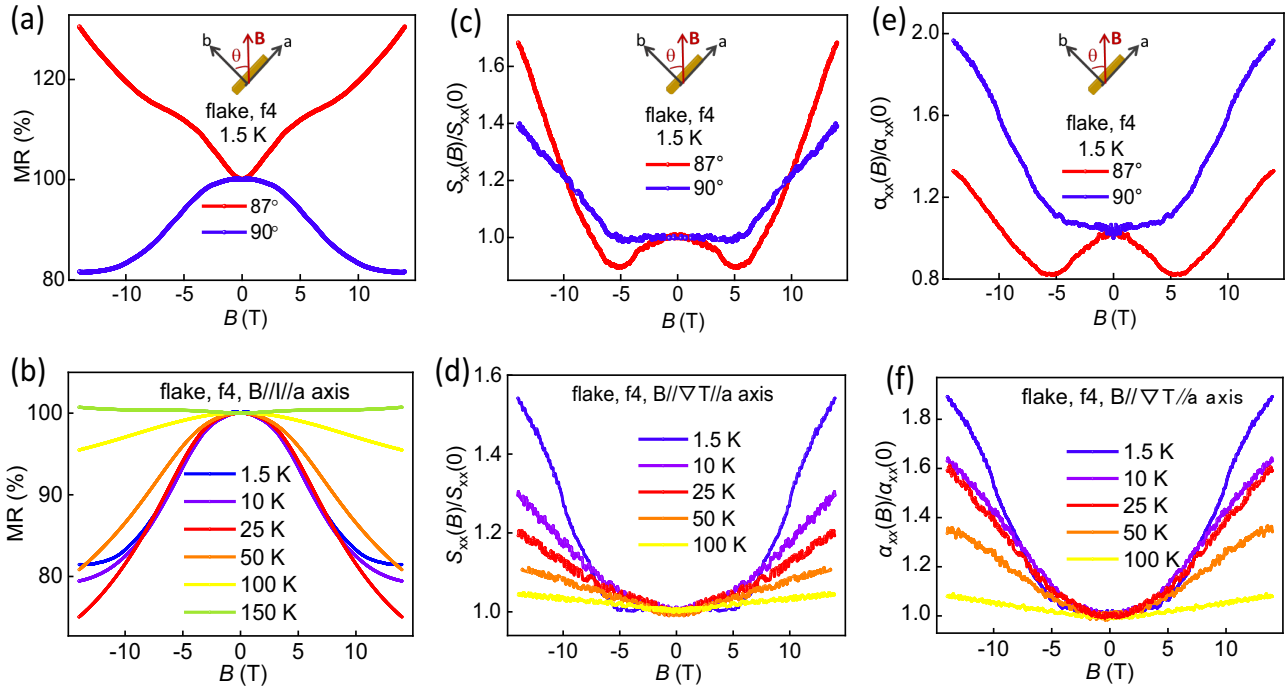

FIG. 3. Negative MR and positive MTP in $ZrTe_5$ under parallel magnetic fields ($B//I$ or $B//\nabla T$). (a),(c) Angle dependence of normalized MR and MTP of $ZrTe_5$ thin flakes near the parallel magnetic fields. (b),(d) Temperature dependence of the normalized MR and MTP of $ZrTe_5$ thin flakes under parallel fields. (e),(f) Angle dependence and temperature dependence of the magnetothermoelectric conductance calculated by the formula $\alpha(B) = S(B)\sigma(B)$.

In another sample (Fig. S7 of the Supplemental Material [41]), we observe clear positive MTP under parallel fields in the whole field range. As shown in Fig. S7, when the orientation of the magnetic field is 3° away from the in-plane direction ($\theta = 87°$), negative MTP is observed at low fields while the MTP remains positive field dependence at high fields. This demonstrates that slight misalignment in the measurements of parallel field configuration significantly influences the low-field MTP result but barely change the high-field behavior. The amplitude of the positive MTP also decreases gradually with increasing temperature and survives up to 100 K [Fig. 3(d)]. The longitudinal magnetothermoelectric conductance of the material is calculated based on the formula $\alpha(B) = S(B)\sigma(B)$ and shown in Figs. 3(e) and 3(f). Here, $\alpha(B)$ denotes the magnetothermoelectric conductance. Thus, in addition to the positive longitudinal magnetoconductance, we also unveil a positive longitudinal magnetothermoelectric conductance with a similar temperature and angle dependence as the positive MTP.

IV. THEORETICAL ANALYSIS AND DISCUSSION

Figures 2 and 3 show that we have detected rather anomalous magnetothermoelectric behavior in the flux-grown $ZrTe_5$. Recent studies of bulk crystals and flakes (a few hundred nanometers thick) have shown that $ZrTe_5$ is a massive Dirac material which holds three-dimensional massive Dirac fermions with nearly linear bulk band dispersion and a band gap [21,47]. To interpret the results, we use the massive Dirac model which has been effectively used to describe $ZrTe_5$ in previous studies [21]. Previous magnetoinfrared spectroscopy measurements suggest that the quantum limit of flux-grown $ZrTe_5$ bulk crystals and thin flakes is lower than 1 T [20,48]. In our measurements, the maximum magnetic field is 33 T and thus we focus on the quantum transport and scattering mechanism beyond the quantum limit. In perpendicular magnetic fields, the longitudinal conductivity σ_{xx} from the zeroth Landau level is related to the relaxation times $\tau_{1s\lambda}$, which arises from the virtual scattering processes between the zeroth Landau band E_{0+} and the first Landau bands $E_{1s\lambda}$. σ_{xx} is then given by [49,50]

$$\sigma_{xx} \simeq \frac{\hbar e^2}{2\pi}\frac{1}{2\ell_B^2}\int_{-\infty}^{\infty} d\varepsilon\left[-\frac{\partial n_F(\varepsilon)}{\partial\varepsilon}\right] \times \sum_{s,\lambda,k_z}\left[\left(v^x_{0,1s\lambda}\right)^2 \frac{\frac{\hbar}{2\tau_{1s\lambda}}}{(\varepsilon - E_{1s\lambda})^2 + \left(\frac{\hbar}{2\tau_{1s\lambda}}\right)^2}\delta(\varepsilon - E_{0+})\right]. \quad (1)$$

Here $\ell_B = \sqrt{\hbar/eB}$ is the magnetic length and $n_F(\varepsilon)$ is the Fermi distribution function. The velocity element $v^x_{0,1s\lambda}$ couples the zeroth band and bands $1s\lambda$. In perpendicular magnetic fields, we also need to consider the Hall conductivity. Then, the resistivity and the Seebeck coefficient are given by $\rho_{xx} = \sigma_{xx}/(\sigma_{xx}^2 + \sigma_{xy}^2)$ and

$$S_{xx} = \frac{\pi^2 k_B^2 T}{3e}\frac{1}{\sigma_{xx}^2 + \sigma_{xy}^2}\left(\sigma_{xx}\frac{\partial\sigma_{xx}}{\partial E_F} + \sigma_{xy}\frac{\partial\sigma_{xy}}{\partial E_F}\right). \quad (2)$$

The relaxation time $\tau_{1s\lambda}$ depends on the electron-impurity scattering and can be calculated in the Born approximation

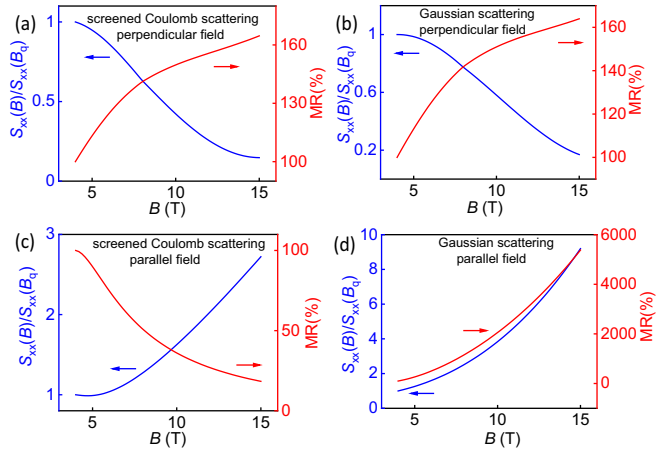

FIG. 4. MR and MTP calculated using the massive Dirac model and different scattering potentials. The MR and MTP are normalized with respect to the value at B_q (quantum limit). (a),(c) The results calculated using the long-range screened Coulomb scattering. A negative MTP and a positive MR are obtained under the perpendicular field, while a positive MTP and a negative MR are obtained under the parallel field, consistent with the experimental observations. (b),(d) The results calculated using the Gaussian scattering. The MR is positive for the parallel field case, contrary to the experimental observations.

[49,50] as

$$\frac{\hbar}{\tau_{1s\lambda}} = \pi n_i \ell_B^2 \sum_{k_z'} \left(F^{1s\lambda,0}_{k_z,k_z'}\right)^2 \times \sum_{\boldsymbol{q}} |u(\boldsymbol{q})|^2 q_\perp^2 \, e^{-\ell_B^2 q_\perp^2/2} \delta_{q_z,k_z-k_z'} \delta\left(\varepsilon - E^{k_z'}_{0+}\right). \quad (3)$$

Here, n_i is the impurity density, $F^{1s\lambda,0}_{k_z,k_z'}$ is a form factor, $u(\boldsymbol{q})$ is the Fourier transformation of the scattering potential, $q_\perp^2 = q_x^2 + q_y^2$, and $E^{k_z'}_{0+} = \sqrt{v^2(k_z')^2 + (b_z - m)^2}$ is the energy dispersion of the lowest Landau band with v the Fermi velocity, b_z the Zeeman splitting energy, and m the gap.

It is known that the impurity scattering potential could strongly influence the thermoelectric transport behavior. We have examined two typical scattering potentials, the screened Coulomb potential induced by charged impurities and the Gaussian scattering potential induced by neutral impurities. Since the anomalous thermoelectric behavior is stronger at low temperature, scattering from phonons is excluded from our analyses. The screened Coulomb potential of charged impurities is $U(\boldsymbol{r}) \propto \sum_i e^{-\kappa|\boldsymbol{r}-\boldsymbol{R}_i|}/|\boldsymbol{r}-\boldsymbol{R}_i|$, while the random Gaussian scattering potential from the neutral impurities is $U(\boldsymbol{r}) \propto \sum_i e^{-|\boldsymbol{r}-\boldsymbol{R}_i|^2/2d^2}$. Here, $\boldsymbol{R}_i$ is the position of a randomly distributed impurity, $1/\kappa$ is the screening length for screened Coulomb potential, and d is the acting range of the impurity potential for Gaussian potential. Our calculations [Figs. 4(a) and 4(b)] reveal that both scatterings yield positive MR and negative MTP as observed in the experiments when the potentials are long ranged under the perpendicular field, that is, $1/\kappa, d > \ell_B$ (see Part II of the Supplemental Material for more details [41]).

In a parallel field, the conductivity is related to the diagonal element of the velocity and the vertex correction of the velocity element should be considered. After vertex correction, the relaxation time is corrected to the transport time [51,52], giving the following formula:

$$\sigma_{xx} = \frac{e^2}{h} \frac{1}{2\pi\ell_B^2} \frac{v^2 k_F}{E_F} \left(\frac{\tau^{\rm tr}_{k_F}}{\hbar} + \frac{\tau^{\rm tr}_{-k_F}}{\hbar}\right). \quad (4)$$

The transport time at the Fermi energy E_F is given by

$$\frac{\hbar}{\tau^{\rm tr}_{\pm k_F}} = \frac{2E_F}{v^2 k_F} n_i \cos^2\left[\frac{1}{2}(\alpha_{k_F} - \alpha_{-k_F})\right] \times \sum_{q_y,q_z} |u(\pm 2k_F, q_y, q_z)|^2 \, e^{-(q_y^2+q_z^2)\ell_B^2/2} \quad (5)$$

with $\alpha_{\pm k_F} = \mp \tan^{-1}[v k_F/(b_x + m)]$, k_F the Fermi wave vector, and b_x the Zeeman energy. The resistivity is the inverse of the conductivity and the Seebeck response can be obtained through the Mott relation. The transport time strongly relies on the scattering potential, which results in various magnetic-field dependencies for various scattering types. In particular, the resistivity due to the Gaussian potential at fixed carrier density is given by

$$\rho_{xx} = \frac{h}{e^2} \frac{n_i u_0^2}{v^2} \frac{(b_x + m)^2}{4\pi^4 v^2 n^2 \ell_B^2 (2d^2 + \ell_B^2)} e^{-16\pi^4 n^2 \ell_B^4 d^2}. \quad (6)$$

Since b_x increases with the magnetic field, while l_B decreases, ρ_{xx} always increases with the field for arbitrary acting ranges [Fig. 4(d)], conflicting with the experimental results. However, the screened Coulomb scattering potential can lead to positive MTP and negative MR regardless of screening length in parallel fields [Fig. 4(c) and Fig. S10 of the Supplemental Material [41]], consistent with our observations. This parallel field case is completely distinct from the perpendicular one. In perpendicular magnetic field, the in-plane motion is quantized and the in-plane momentum is not a good quantum number. The velocity is off diagonal. The conductivity relates to the higher-order off-diagonal velocity element, which leads to the virtual process going back and forth between the zeroth band and the nearest high band [49]. The conductivity is almost inversely proportional to the relaxation time. Further, the Hall conductivity also influences the magnetoresistance and the Seebeck coefficient in the perpendicular field case. Combining the calculations and experimental results, we qualitatively attribute the observed anomalous MTP and MR phenomena to the transport behavior in the presence of long-range screened Coulomb potential. More details of the calculations are shown in the Supplemental Material [41].

In the quantum limit, all the electrons occupy the lowest Landau band. This band is affected by the external magnetic field. In contrast to the classical case, the transport time or the relaxation time of this one-band quantum system is strongly influenced by the magnetic field and the scattering potential. Therefore, the transport behavior in the quantum limit is very sensitive to the scattering mechanism. As shown by the calculations, impurity scattering strongly influences the relaxation time (perpendicular field configuration) or transport time (parallel field configuration) in massive Dirac materials, which determines the magnetotransport properties. In the $ZrTe_5$ samples grown by the IVT method, the MTP shows a nonmonotonic field dependence in the perpendicular field and a negative field dependence in the parallel field [53,54].

The difference in thermoelectric transport behavior between IVT-grown $ZrTe_5$ and flux-grown $ZrTe_5$ may originate from the different impurity scattering potentials formed during the growth process. Furthermore, our results suggest a need for caution in interpreting a negative MR under a parallel magnetic field as the signature of a chiral anomaly in Dirac materials [1] or helicity transport in massive Dirac materials [55–58]. Our studies indicate that impurity scattering should also be taken into serious consideration in the understanding of the anomalous transport behaviors.

V. CONCLUSION

In conclusion, we observed anomalous magnetothermoelectric transport behavior in thin flakes of massive Dirac material $ZrTe_5$. We found a large negative MTP in a perpendicular field while the MTP was positive in a parallel field. The MTP behavior is distinct from the generally expected results in Dirac materials although the observed MR shows a field dependence consistent with previous reports. This exotic behavior can be qualitatively explained by the long-range screened Coulomb scattering potential in the quantum limit of a massive Dirac band structure. The combined angle-dependent electrical and thermoelectric transport studies presented in this work provide important insights into quantum transport phenomena in topological materials.

ACKNOWLEDGMENTS

We thank X. Qiang and C. Xi for helpful discussions. J.W. acknowledges the National Key R&D Program of China (Grant No. 2018YFA0305604), Beijing Natural Science Foundation (Grant No. Z180010), the National Natural Science Foundation of China (Grant No. 11888101), the Innovation Program for Quantum Science and Technology (Grant No. 2021ZD0302400), and the Strategic Priority Research Program of Chinese Academy of Sciences (Grant No. XDB28000000). X.W. acknowledges the support from the National Key Basic Research R&D Program of China (Grant No. 2020YFA0308800) and the National Natural Science Foundation of China (Grants No. 11774009 and No. 12074009). H.L. acknowledges the National Natural Science Foundation of China (Grant No. 11925402), Guangdong province (Grants No. 2016ZT06D348 and No. 2020KCXTD001), Shenzhen High-level Special Fund (Grants No. G02206304 and G02206404), and the Science, Technology and Innovation Commission of Shenzhen Municipality (Grants No. ZDSYS20170303165926217, No. JCYJ20170412152620376, and No. KYTDPT20181011104202253), and Center for Computational Science and Engineering of SUSTech. H.W. acknowledges the National Natural Science Foundation of China (Grants No. 21BAA01133, No. 12004441, and No. 92165204), the Hundreds of Talents program of Sun Yat-sen University and the Fundamental Research Funds for the Central Universities (Grant No. 202lqntd27). C.W. acknowledges the National Natural Science Foundation of China (Grant No. 11974249) and the Natural Science Foundation of Shanghai (Grant No. 19ZR1437300). J.Y. and D.M. acknowledge the U.S. Department of Energy, Office of Science, Basic Energy Sciences, Materials Sciences and Engineering Division. J.D. acknowledges the support from Guangdong-Hong Kong-Macao Joint Laboratory for Photonic-Thermal-Electrical Energy Materials and Devices (GDSTC No. 2019B121205001).

Y.L., H.W., Jingyue W., and C.W. contributed equally to this work.

[1] Z. Jia, C. Li, X. Li, J. Shi, Z. Liao, D. Yu, and X. Wu, Nat. Commun. **7**, 13013 (2016).
[2] M. Hirschberger, S. Kushwaha, Z. Wang, Q. Gibson, S. Liang, C. A. Belvin, B. A. Bernevig, R. J. Cava, and N. P. Ong, Nat. Mater. **15**, 1161 (2016).
[3] T. Liang, Q. Gibson, J. Xiong, M. Hirschberger, S. P. Koduvayur, R. J. Cava, and N. P. Ong, Nat. Commun. **4**, 2696 (2013).
[4] B. Skinner and L. Fu, Sci. Adv. **4**, eaat2621 (2018).
[5] J. M. Ziman, *Electrons and Phonons* (Clarendon Press, Oxford, 1960), p. 500.
[6] B. Skinner, T. Chen, and B. I. Shklovskii, J. Exp. Theor. Phys. **117**, 579 (2013).
[7] H. Beidenkopf, P. Roushan, J. Seo, L. Gorman, I. Drozdov, Y. S. Hor, R. J. Cava, and A. Yazdani, Nat. Phys. **7**, 939 (2011).
[8] B. Skinner, Phys. Rev. B **90**, 060202(R) (2014).
[9] J. Klier, I. V. Gornyi, and A. D. Mirlin, Phys. Rev. B **92**, 205113 (2015).
[10] S. Das Sarma, E. H. Hwang, and H. Min, Phys. Rev. B **91**, 035201 (2015).
[11] D. A. Pesin, E. G. Mishchenko, and A. Levchenko, Phys. Rev. B **92**, 174202 (2015).
[12] S. Das Sarma and E. H. Hwang, Phys. Rev. B **91**, 195104 (2015).
[13] H.-Z. Lu and S.-Q. Shen, Front. Phys. **12**, 127201 (2017).
[14] R. Takahashi and S. Murakami, Semicond. Sci. Technol. **27**, 124005 (2012).
[15] R. Lundgren, P. Laurell, and G. A. Fiete, Phys. Rev. B **90**, 165115 (2014).
[16] Q. Chen and G. A. Fiete, Phys. Rev. B **93**, 155125 (2016).
[17] A. Pariari, N. Khan, R. Singha, B. Satpati, and P. Mandal, Phys. Rev. B **94**, 165139 (2016).
[18] V. Könye and M. Ogata, Phys. Rev. B **100**, 155430 (2019).
[19] L. X. Fu and C. M. Wang, Phys. Rev. B **105**, 035201 (2022).
[20] Y. Jiang, Z. L. Dun, H. D. Zhou, Z. Lu, K. W. Chen, S. Moon, T. Besara, T. M. Siegrist, R. E. Baumbach, D. Smirnov, and Z. Jiang, Phys. Rev. B **96**, 041101(R) (2017).
[21] Z.-G. Chen, R. Y. Chen, R. D. Zhong, J. Schneeloch, C. Zhang, Y. Huang, F. Qu, R. Yu, Q. Li, G. D. Gu, and N. L. Wang, Proc. Natl. Acad. Sci. USA **114**, 816 (2017).
[22] Y. Zhang, C. Wang, L. Yu, G. Liu, A. Liang, J. Huang, S. Nie, X. Sun, Y. Zhang, B. Shen, J. Liu, H. Weng, L. Zhao, G. Chen, X. Jia, C. Hu, Y. Ding, W. Zhao, Q. Gao, C. Li *et al.*, Nat. Commun. **8**, 15512 (2017).

[23] Y. Liu, X. Yuan, C. Zhang, Z. Jin, A. Narayan, C. Luo, Z. Chen, L. Yang, J. Zou, X. Wu, S. Sanvito, Z. Xia, L. Li, Z. Wang, and F. Xiu, Nat. Commun. **7**, 12516 (2016).

[24] X.-B. Li, W.-K. Huang, Y.-Y. Lv, K.-W. Zhang, C.-L. Yang, B.-B. Zhang, Y. B. Chen, S.-H. Yao, J. Zhou, M.-H. Lu, L. Sheng, S.-C. Li, J.-F. Jia, Q.-K. Xue, Y.-F. Chen, and D.-Y. Xing, Phys. Rev. Lett. **116**, 176803 (2016).

[25] R. Wu, J. Z. Ma, S. M. Nie, L. X. Zhao, X. Huang, J. X. Yin, B. B. Fu, P. Richard, G. F. Chen, Z. Fang, X. Dai, H. M. Weng, T. Qian, H. Ding, and S. H. Pan, Phys. Rev. X **6**, 021017 (2016).

[26] G. Manzoni, L. Gragnaniello, G. Autès, T. Kuhn, A. Sterzi, F. Cilento, M. Zacchigna, V. Enenkel, I. Vobornik, L. Barba, F. Bisti, P. Bugnon, A. Magrez, V. N. Strocov, H. Berger, O. V. Yazyev, M. Fonin, F. Parmigiani, and A. Crepaldi, Phys. Rev. Lett. **117**, 237601 (2016).

[27] H. Wang, H. Liu, Y. Li, Y. Liu, J. Wang, J. Liu, J.-Y. Dai, Y. Wang, L. Li, J. Yan, D. Mandrus, X. C. Xie, and J. Wang, Sci. Adv. **4**, eaau5096 (2018).

[28] H. Wang, Y. Liu, Y. Liu, C. Xi, J. Wang, J. Liu, Y. Wang, L. Li, S. P. Lau, M. Tian, J. Yan, D. Mandrus, J.-Y. Dai, H. Liu, X. Xie, and J. Wang, Natl. Sci. Rev. **6**, 914 (2019).

[29] Y. Liu, H. Wang, H. Zhu, Y. Li, J. Ge, J. Wang, L. Li, J.-Y. Dai, J. Yan, D. Mandrus, R. Joynt, and J. Wang, npj Quantum Mater. **5**, 88 (2020).

[30] F. Tang, Y. Ren, P. Wang, R. Zhong, J. Schneeloch, S. A. Yang, K. Yang, P. A. Lee, G. Gu, Z. Qiao, and L. Zhang, Nature (London) **569**, 537 (2019).

[31] W. Zhang, P. Wang, B. Skinner, R. Bi, V. Kozii, C.-W. Cho, R. Zhong, J. Schneeloch, D. Yu, G. Gu, L. Fu, X. Wu, and L. Zhang, Nat. Commun. **11**, 1046 (2020).

[32] Q. Li, D. E. Kharzeev, C. Zhang, Y. Huang, I. Pletikosić, A. V. Fedorov, R. D. Zhong, J. A. Schneeloch, G. D. Gu, and T. Valla, Nat. Phys. **12**, 550 (2016).

[33] Z. Sun, Z. Cao, J. Cui, C. Zhu, D. Ma, H. Wang, W. Zhuo, Z. Cheng, Z. Wang, X. Wan, and X. Chen, npj Quantum Mater. **5**, 36 (2020).

[34] T. Liang, J. Lin, Q. Gibson, S. Kushwaha, M. Liu, W. Wang, H. Xiong, J. A. Sobota, M. Hashimoto, P. S. Kirchmann, Z.-X. Shen, R. J. Cava, and N. P. Ong, Nat. Phys. **14**, 451 (2018).

[35] J. Mutch, X. Ma, C. Wang, P. Malinowski, J. Ayres-Sims, Q. Jiang, Z. Liu, D. Xiao, M. Yankowitz, and J.-H. Chu, arXiv:2101.02681.

[36] J. Ge, D. Ma, Y. Liu, H. Wang, Y. Li, J. Luo, T. Luo, Y. Xing, J. Yan, D. Mandrus, H. Liu, X. C. Xie, and J. Wang, Natl. Sci. Rev. **7**, 1879 (2020).

[37] J. P. Small, K. M. Perez, and P. Kim, Phys. Rev. Lett. **91**, 256801 (2003).

[38] Y. M. Zuev, W. Chang, and P. Kim, Phys. Rev. Lett. **102**, 096807 (2009).

[39] J. Gooth, A. C. Niemann, T. Meng, A. G. Grushin, K. Landsteiner, B. Gotsmann, F. Menges, M. Schmidt, C. Shekhar, V. Süß, R. Hühne, B. Rellinghaus, C. Felser, B. Yan, and K. Nielsch, Nature (London) **547**, 324 (2017).

[40] P. Shahi, D. J. Singh, J. P. Sun, L. X. Zhao, G. F. Chen, Y. Y. Lv, J. Li, J. Q. Yan, D. G. Mandrus, and J. G. Cheng, Phys. Rev. X **8**, 021055 (2018).

[41] See Supplemental Material at http://link.aps.org/supplemental/10.1103/PhysRevB.107.085140, which includes Refs. [20,21,23,48–52,56–58], for details.

[42] J. Niu, J. Wang, Z. He, C. Zhang, X. Li, T. Cai, X. Ma, S. Jia, D. Yu, and X. Wu, Phys. Rev. B **95**, 035420 (2017).

[43] G. N. Kamm, D. J. Gillespie, A. C. Ehrlich, T. J. Wieting, and F. Levy, Phys. Rev. B **31**, 7617 (1985).

[44] N. P. Ong and S. Liang, Nat. Rev. Phys. **3**, 394 (2021).

[45] G. Zheng, J. Lu, X. Zhu, W. Ning, Y. Han, H. Zhang, J. Zhang, C. Xi, J. Yang, H. Du, K. Yang, Y. Zhang, and M. Tian, Phys. Rev. B **93**, 115414 (2016).

[46] J. Wang, J. Niu, B. Yan, X. Li, R. Bi, Y. Yao, D. Yu, and X. Wu, Proc. Natl. Acad. Sci. USA **115**, 9145 (2018).

[47] J. Mutch, W.-C. Chen, P. Went, T. Qian, I. Z. Wilson, A. Andreev, C.-C. Chen, and J.-H. Chu, Sci. Adv. **5**, eaav9771 (2019).

[48] R. Y. Chen, Z. G. Chen, X. Y. Song, J. A. Schneeloch, G. D. Gu, F. Wang, and N. L. Wang, Phys. Rev. Lett. **115**, 176404 (2015).

[49] H.-Z. Lu, S.-B. Zhang, and S.-Q. Shen, Phys. Rev. B **92**, 045203 (2015).

[50] S.-B. Zhang, H.-Z. Lu, and S.-Q. Shen, New J. Phys. **18**, 053039 (2016).

[51] H. Bruus and K. Flensberg, *Many-Body Quantum Theory in Condensed Matter Physics: An Introduction* (Oxford Graduate Texts, Oxford, 2004).

[52] Y. Chen, H.-Z. Lu, and X. C. Xie, Phys. Rev. Lett. **121**, 036602 (2018).

[53] W. Zhang, P. Wang, G. Gu, X. Wu, and L. Zhang, Phys. Rev. B **102**, 115147 (2020).

[54] J. L. Zhang, C. M. Wang, C. Y. Guo, X. D. Zhu, Y. Zhang, J. Y. Yang, Y. Q. Wang, Z. Qu, L. Pi, H.-Z. Lu, and M. L. Tian, Phys. Rev. Lett. **123**, 196602 (2019).

[55] A. V. Andreev and B. Z. Spivak, Phys. Rev. Lett. **120**, 026601 (2018).

[56] A. A. Abrikosov, Phys. Rev. B **58**, 2788 (1998).

[57] E. H. Hwang and S. Das Sarma, Phys. Rev. B **79**, 165404 (2009).

[58] A. B. Pippard, *Magnetoresistance in Metals* (Cambridge University Press, New York, 1989).